

Sketch2Colab: Sketch-Conditioned Multi-Human Animation via Controllable Flow Distillation

Divyanshu Daiya Aniket Bera

IDEAS Lab, Department of Computer Science, Purdue University

divyanshu@purdue.edu, aniketbera@purdue.edu



Figure 1. **Sketch-conditioned human-object-human (HOH) demonstrations with Sketch2Colab.** Left→right: **(a)** Two people co-manipulate a table while following a sketched path; midway the model *switches handling* so that one character disengages and the other finishes the placement, showing that Sketch2Colab can start/stop agent motion based on joint/body trajectory cues. **(b)** Cooperative transport of a large box along a prescribed trajectory with *on-the-fly height adjustment* before placing it down. **(c)** A specified hand must grasp a canister and then follow a *complex path*. In all cases, the system is driven only by sparse storyboard keyframes (no text conditioning); the generated motions respect the keyframe timing, the requested joint/endpoint trajectories, and object alignment/contacts.

Abstract

We present Sketch2Colab, which turns storyboard-style 2D sketches into coherent, object-aware 3D multi-human motion with fine-grained control over agents, joints, timing, and contacts. Conventional diffusion-based motion generators have advanced realism; however, achieving precise adherence to rich interaction constraints typically demands extensive training and/or costly posterior guidance, and performance can degrade under strong multi-entity conditioning. Sketch2Colab instead first learns a sketch-driven diffusion prior and then distills it into an efficient rectified-flow student operating in latent space for fast, stable sampling. Differentiable energies over keyframes, trajectories, and physics-based constraints directly shape the student’s transport field, steering samples toward motions that faithfully satisfy the storyboard while remaining physically plausible. To capture coordinated interaction, we augment the continuous flow with a continuous-time Markov chain (CTMC) planner that schedules discrete events such as touches, grasps, and handoffs, modulating the dynamics to produce crisp, well-phased human-object-human collaborations. Experiments on CORE4D and InterHuman show that Sketch2Colab achieves state-of-the-art constraint adherence and perceptual quality while offering significantly

faster inference than diffusion-only baselines.

1. Introduction

Creating believable multi-entity motion is a persistent labor intensive bottleneck in game development, film, and VR/AR. Complex scenes—where multiple humans coordinate while interacting with objects—are still largely crafted by hand, requiring animators to iterate for hours to remove jitter, resolve collisions, and refine timing, or to rely on motion capture pipelines that are difficult to scale across the combinatorics of tasks and layouts [24, 57]. In parallel, generative motion modeling has progressed rapidly: text-conditioned generation [12, 32, 55, 57, 69], trajectory/pose-conditioned control and editing [4, 15, 34, 50, 61, 64], and style transfer [1, 52, 71] have all seen strong results in single-human and, more recently, multi-human or human-scene settings [16, 17, 21, 29, 33, 44, 62]. Yet, in truly multi-entity scenarios—where several agents must coordinate with shared objects and follow rich task constraints—there remain comparatively few methods. One notable exception is COLLAGE [17], which couples LLM-based planning with a latent diffusion generator to follow complex textual instructions in human-object-human (HOH) interactions.

While text is convenient for planning, it is often an

inarticulate control channel: timing, phasing, and spatial layout are more naturally conveyed by visual cues such as keyframes, coarse joint trajectories, and object paths. Sketch-based interfaces therefore provide a compelling alternative. SKETCH2ANIM [70] demonstrates that storyboard keyposes and joint/endpoint trajectories can effectively constrain a diffusion model to produce a single-human motion consistent with the artist’s intent. However, [70] focuses on one character and does not model inter-agent coordination, hand–object contacts, or collision-free co-manipulation. In this work we ask: *how can we extend sketch-driven control to multi-human, object-centric interactions with coupled constraints?*

Diffusion models are the de facto backbone for motion generation due to their sample quality and data efficiency [13, 18, 27, 51, 57]. Yet achieving *precise* constraint following typically requires task-specific guidance (e.g., posterior guidance) or specialized control modules at inference, which can cause sampling slowdowns, lagging responses to hard constraints, or mode bias toward easy-to-satisfy solutions [14, 15, 64, 71]. Recent evidence suggests that *flow-based* generators—particularly rectified/conditional flow matching—can offer more direct transport between source and target distributions, with improved stability under strong conditioning and faster sampling [20, 25, 42, 43]. MotionLab [25] leverages rectified flows to unify generation and editing tasks, reporting stronger alignment without expensive posterior guidance; similar trends appear in non-motion domains where flow-based samplers better respect structured constraints or inverse-problem likelihoods [2, 8].

A straightforward idea, then, is to translate sketch-conditioned diffusion methods (e.g., COLLAGE-style latent diffusion [17] or SKETCH2ANIM [70]) into a multi-entity *flow* generator that ingests multi-track keyframes and joint/object trajectories. However, in our experiments, directly scaling diffusion baselines to multi-entity sketches produced suboptimal adherence: keyframe misalignments, inter-agent phase drift, and noticeable jitter or lag relative to the target trajectories. Training a competitive flow model *from scratch* for interactive HOH scenarios is also challenging and compute-intensive, as the model must learn a transport field that simultaneously handles multi-agent timing, contacts, and mutual constraints [2, 42, 43]. To address this, we adopt a diffusion-to-flow *distillation* strategy, initializing a rectified-flow student from a strong sketch-driven diffusion teacher, akin to recent distillation approaches for accelerating conditional sampling [8, 20, 25].

Distillation alone is not sufficient: if the diffusion teacher only weakly satisfies constraints, the student can inherit the same failure modes. We therefore augment the student with *energy-based* guidance that explicitly shapes the data manifold toward constraint satisfaction. Inspired by

recent energy-matching perspectives [6] and classical EBM conditioning [19, 53], we define differentiable energies for keyframe pose fidelity, joint/endpoint trajectory tracking, inter-agent/object distances, contact consistency, and collision penalties. During training and sampling, the rectified flow follows transport directions that are jointly informed by the distilled velocity field and the gradients of these energies, improving adherence without requiring slow posterior guidance loops [8, 14].

Finally, multi-entity interaction involves *discrete* latent events (contact on/off, grasp state, object handoffs) whose schedules are difficult to optimize via purely continuous flows. We introduce a lightweight *CTMC-based* planner over these discrete states, learned with a physics-informed objective inspired by non-equilibrium transport samplers for discrete distributions [28]. The CTMC proposes contact/handoff schedules consistent with the sketch, while the continuous rectified flow handles pose-level transport; importance-weighted coupling aligns the two, reducing mode switches, temporal lag, and contact flicker.

Contributions. We present a sketch-conditioned, multi-entity motion generator *Sketch2Colab* for collaborative HOH scenarios that:

- Distills a rectified-flow student from a strong sketch-driven diffusion teacher to obtain fast, stable transport under complex conditioning.
- Introduces *energy-guided rectified flows* for multi-entity motion: differentiable energies enforce keyframe/trajectory constraints, contacts, and collision-avoidance, improving alignment without posterior guidance [6, 14, 19].
- Integrates a *CTMC-based* discrete-event planner for contact and handoff scheduling, coupled to the continuous flow via importance reweighting for robust multi-agent coordination.
- Achieves state-of-the-art constraint adherence and perceptual quality on multi-human, object-centric tasks, while sampling substantially faster than diffusion-only baselines.

2. Related Work

Text-, Trajectory-, and Style-Conditioned Motion. Early work studied action-category and past-motion conditioning [3, 7, 11, 23, 37, 45, 48, 66]. Modern diffusion/GPT-style models enable text-to-motion [12, 32, 55, 57, 68, 69], trajectory control/editing [4, 15, 34, 50, 61, 64], and style transfer [1, 52, 71], and have been extended to multi-person [21, 44, 62] and human–scene/HOI contexts [16, 29, 33, 38, 39]. Our work targets multi-entity, collaborative HOH settings where multiple agents and shared objects must follow coupled constraints. **Collaborative HOH and LLM-Guided Planning.** Recent efforts begin to address collaborative human–object–human interactions. COLLAGE [17] lever-

ages LLM planning [30, 35, 46, 59] with latent diffusion to follow rich text prompts for multi-agent collaboration, and evaluates on datasets such as CORE-4D and InterGen [40, 67]. While text offers global task structure, it under-specifies precise timing and spatial alignment; our approach complements text with visual sketch constraints that tightly specify poses and trajectories.

Sketch- and Keyframe-Driven Animation. Storyboard sketches naturally encode keyposes and joint/endpoint trajectories [36, 63]. Early sketch-to-pose work addressed static posing from stick figures or silhouettes [9, 10, 26, 41], while retrieval and interface-based methods guided motion with path sketches but were limited by database coverage [22, 31, 58, 65]. SKETCH2ANIM [70] introduced multi-conditional diffusion with 2D/3D keyposes and trajectories, but only for single-human motions. We extend the sketch paradigm to multi-entity HOH generation with explicit inter-agent constraints and object coordination.

Diffusion Control vs. Flow-Based Generators. Diffusion backbones remain dominant for motion generation/editing [13, 32, 57], but precise control relies on posterior guidance [14] or ControlNet-like modules [64, 71], which increase sampling cost and can underperform on hard constraints or multi-track coupling. Rectified/conditional flows [42, 43] and DiT-style architectures [20] enable direct transport, improving stability under strong conditions. MotionLab [25] demonstrates that rectified flows can unify generation/editing tasks with strong conditional alignment. Several works have further accelerated conditional sampling by distilling diffusion trajectories into feed-forward transport fields [8, 20]. We follow this direction, using a sketch-driven diffusion teacher to supervise a rectified-flow student in latent motion space, trading sampling steps for a single learned transport while providing fine-control.

Energy-Based Guidance for Constraints. Energy-based models define unnormalized densities that can encode structured priors [19], and recent formulations link flows and EBMs via energy matching on/near the data manifold [6]. We embed energies for keyframes, trajectories, contact consistency, and collision avoidance into both the rectified-flow objective and the sampler, using their gradients to improve adherence without slow posterior guidance loops [14].

Discrete Event Scheduling via CTMCs. Realistic collaboration involves discrete latent events (contacts, grasps, handoffs) whose schedules interact with continuous motion. Continuous-time Markov chains (CTMCs) provide a natural mechanism for such processes and can be learned with non-equilibrium transport objectives and importance weighting [28]. We couple a lightweight CTMC over interaction states with our continuous rectified flow, aligning contact/handoff timing with keyframe/trajectory constraints for robust multi-agent coordination.

Compared to purely text-driven pipelines [17] or single-

human sketch guidance [70], our approach brings sketch-conditioned *multi-entity* control to HOH by combining diffusion-to-flow distillation [8, 20, 25, 42, 43], energy-based constraint shaping [6, 19], and CTMC-driven discrete scheduling [28]. Additional preliminaries (notation, rectified flows, CTMCs, and energies) appear in the Supplementary (Supp. Sec. 2); below we detail our model.

3. Method

We synthesize an N -frame, temporally coherent 3D motion sequence for a scene with H humans and O objects, driven by a storyboard of K keyframes and optional text. From the storyboard we first extract the 2D control signals: for each human h we obtain keyposes at annotated times $\mathcal{T}_{\text{key}} \subset \{1, \dots, N\}$ as $\mathbf{K}_{2\text{D}}^{(h)}[t] \in \mathbb{R}^{J \times 2}$ (pixel coordinates), and, when provided, per-joint 2D polylines describing target image-plane trajectories $\mathbf{T}_{2\text{D}}^{(h,j)} \in \mathbb{R}^{L_{h,j} \times 2}$ with vertex count $L_{h,j}$; for objects we use binary silhouettes or coarse masks $\mathbf{S}_{2\text{D}}^{(o)}[t] \in \{0, 1\}^{H_s \times W_s}$ to indicate placement and extent; an optional free-form text prompt is denoted by \mathbf{a} . We group these conditioning signals as $\mathcal{C} = (\mathbf{K}_{2\text{D}}, \mathbf{T}_{2\text{D}}, \mathbf{S}_{2\text{D}}, \mathbf{a})$ and maintain an elementwise conditioning indicator $\chi \in \{0, 1\}^{N \times (H \cdot J + \sum_o K_o)}$ that specifies, at each frame, which human joints or object anchors are constrained. We denote discrete time by $t \in \{1, \dots, N\}$ and write the full scene state at time t as $\mathbf{M}_t = \mathbf{M}_t^{\text{hum}} \cup \mathbf{M}_t^{\text{obj}}$. For each human $h \in \{1, \dots, H\}$ we track a kinematic skeleton with $J=22$ SMPL-X joints [47]; joint positions are $\mathbf{P}_t^{(h)} \in \mathbb{R}^{J \times 3}$ in a world frame with ground plane $z=0$, and joint orientations use the continuous 6D rotation representation [72] as $\mathbf{R}_t^{(h)} \in \mathbb{R}^{J \times 6}$. For each object $o \in \{1, \dots, O\}$ we store K_o object anchors (e.g., graspable handles or geometric keypoints) as $\mathbf{Y}_t^{(o)} \in \mathbb{R}^{K_o \times 3}$ and a rigid body pose $\mathbf{O}_t^{(o)} \in \mathbb{R}^7$ implemented as 3D translation plus unit quaternion; wherever we refer to “6D rotation” we use the [72] parameterization internally and convert to quaternions for $\mathbf{O}_t^{(o)}$ at decode time. The flattened scene state has dimension,

$$D_{\text{full}} = H \cdot J \cdot (3 + 6) + O \cdot (3 + 4) + \sum_{o=1}^O K_o \cdot 3, \quad (1)$$

so $\mathbf{M}_t \in \mathbb{R}^{D_{\text{full}}}$. We denote the stacked sequence by $\mathbf{M}_{1:N} := [\mathbf{M}_1; \dots; \mathbf{M}_N] \in \mathbb{R}^{N \times D_{\text{full}}}$ and seek to generate this *dense* motion given the *sparse* storyboard controls. Projection to and from the sketch plane follows [70].

Following [17], we operate in a hierarchical VQ-VAE *entity* latent. At level $\ell \in \{1, \dots, L\}$ the frozen encoder outputs continuous latents $\mathbf{z}^{(\ell)} \in \mathbb{R}^{T_{\text{lat}} \times V \times d_\ell}$ and nearest-code indices $\mathbf{c}^{(\ell)} \in \{1, \dots, K_\ell\}^{T_{\text{lat}} \times V}$, where $V = n+m$ is the number of entity tokens (humans and objects) and $T_{\text{lat}} \leq N$ is the latent temporal length after sub-sampling. We aggregate levels into a merged latent $\mathbf{z} \in \mathbb{R}^{T_{\text{lat}} \times V \times d}$ with $d = \sum_{\ell=1}^L d_\ell$ (as in [17]). The frozen decoder $\mathcal{D} : \mathbb{R}^{T_{\text{lat}} \times V \times d} \rightarrow \mathbb{R}^{N \times D_{\text{full}}}$ upsamples temporally and decodes

per-entity motion. Because guidance is defined in motion space but sampling occurs in latent space, we learn a low-rank block-Toeplitz Jacobian surrogate $\mathbf{B}_\rho \approx (\partial\mathcal{D}/\partial\mathbf{z})^\top \in \mathbb{R}^{(T_{\text{lat}} \cdot V \cdot d) \times (N \cdot D_{\text{full}})}$ to precondition gradients stably.

To bridge sketches and 3D Motion, similar to Sketch2Anim[49, 55, 70], we train paired 2D/3D encoders for keyposes, trajectories, and objects, $\{\mathcal{E}_y^{2D}, \mathcal{E}_y^{3D}\}_{y \in \{k, \tau, o\}}$, each mapping their inputs to a shared embedding space \mathbb{R}^{d_e} with $d_e=256$. The alignment loss

$$\mathcal{L}_{\text{align}} = \sum_{y \in \{k, \tau, o\}} \|\mathbf{s}_y^{3D} - \mathbf{s}_y^{2D}\|_2^2 + \lambda_c \mathcal{L}_{\text{InfoNCE}}(y) \quad (2)$$

encourages modality-invariant embeddings by combining an L_2 term and a mini-batch contrastive objective [60]; at inference we retain only 2D branches, feeding the generator via attention and feature adapters described below.

3.1. Generative Field: Diffusion Teacher and Rectified-Flow Student

Both networks share the same backbone: a 4-level temporal U-Net [17, 27] acting on $\mathbf{z} \in \mathbb{R}^{T_{\text{lat}} \times V \times d}$ with temporal convolutions [5], local temporal self-attention (window $w=9$), and an entity-graph attention block whose logits are modulated by metric distances between entity tokens. Let $\mathbf{Q}, \mathbf{K}, \mathbf{V} \in \mathbb{R}^{T_{\text{lat}} \times V \times d_h}$ be head-wise projections and $\mathbf{D} \in \mathbb{R}^{V \times V}$ pairwise distances (zero diagonal), broadcast over time. We apply attention *per t* and stack:

$$\text{Attn}_t = \text{Softmax}\left(\frac{\mathbf{Q}_t \mathbf{K}_t^\top}{\sqrt{d_h}} - \lambda \mathbf{D}\right) \mathbf{V}_t \quad (3)$$

where, $\text{Attn}(\mathbf{Q}, \mathbf{K}, \mathbf{V}; \mathbf{D}) = \text{stack}_{t=1}^{T_{\text{lat}}}(\text{Attn}_t)$. This biases information flow toward spatially proximal agents and object anchors at each time step [17].

Teacher probability flow. We first pre-train the diffusion teacher to convergence and then freeze its parameters θ ; all subsequent supervision uses the teacher’s fixed probability-flow velocity. The diffusion teacher is trained with a variance-preserving (VP) noise schedule [54], $\mathbf{z}_t = \sqrt{\bar{\alpha}_t} \mathbf{z}_0 + \sqrt{1 - \bar{\alpha}_t} \boldsymbol{\epsilon}$ with $\boldsymbol{\epsilon} \sim \mathcal{N}(0, \mathbf{I})$, to predict noise $\hat{\boldsymbol{\epsilon}}_\theta(\mathbf{z}_t, t | \mathcal{C})$. From this we derive a closed-form probability-flow velocity field as,

$$v_\theta^{\text{PF}}(\mathbf{z}_t, t | \mathcal{C}) = \frac{d\bar{\alpha}_t}{dt} \frac{\mathbf{z}_t - \sqrt{1 - \bar{\alpha}_t} \hat{\boldsymbol{\epsilon}}_\theta}{\sqrt{\bar{\alpha}_t}} - \frac{d(1 - \bar{\alpha}_t)}{dt} \frac{\hat{\boldsymbol{\epsilon}}_\theta}{2\sqrt{1 - \bar{\alpha}_t}}, \quad (4)$$

which we use as supervision for the rectified-flow student $v_\phi(\mathbf{z}, t | \mathcal{C}) \in \mathbb{R}^{T_{\text{lat}} \times V \times d}$. The student minimizes the rectified-flow objective[43]

$$\mathcal{L}_{\text{RF}}(\phi) = \mathbb{E}_{t, \mathbf{z}_0, \mathbf{z}_1} \|\mathbf{v}_\phi(\mathbf{z}_t, t | \mathcal{C}) - (\mathbf{z}_1 - \mathbf{z}_0)\|_2^2, \quad (5)$$

here $\mathbf{z}_t = (1 - t)\mathbf{z}_0 + t\mathbf{z}_1$, together with explicit PF-distillation

$$\mathcal{L}_{\text{distill}}(\phi) = \mathbb{E}_{t, \mathbf{z}_t} \|v_\phi(\mathbf{z}_t, t | \mathcal{C}) - v_\theta^{\text{PF}}(\mathbf{z}_t, t | \mathcal{C})\|_2^2, \quad (6)$$

We use a *lift-then-fuse* scheme tailored to storyboard control. The 2D inputs in $\mathcal{C} = (\mathbf{K}_{2D}, \mathbf{T}_{2D}, \mathbf{S}_{2D}, \mathbf{a})$ are mapped via the aligned encoders (Sec. 3.1, Eq. (2)) to

3D proxies $(\hat{\mathbf{K}}_{3D}, \hat{\mathbf{T}}_{3D})$; \mathbf{S}_{2D} is used only for association/scale during this lift. Following [64, 70], we condition the latent U-Net with two routes: (i) a *trajectory path* (ControlNet-style) that injects per-level residuals $\mathbf{r}_\tau^{(\ell)}(t)$ from $\hat{\mathbf{T}}_{3D}$ and, uniquely, adds a temporal attention bias $\mathbf{b}_\tau^{(\ell)}$ computed from along-path phase $\phi(t) = [s(t), \dot{s}(t), \kappa(t)]$ to improve mid-sequence timing; and (ii) a *time-gated keyframe adapter* that applies localized residuals $\mathbf{r}_{\text{KF}}^{(\ell)}(t) = \sum_{t^* \in \mathcal{T}_{\text{key}}} \delta_\sigma(t - t^*) \mathcal{F}_k^{3D}(\hat{\mathbf{K}}_{3D}[t^*])$ to snap poses near key times \mathcal{T}_{key} without disturbing transport elsewhere. Text \mathbf{a} is encoded once and applied by a single bottleneck cross-attention (cf. [17]), as no level-specific semantics are required. Optionally (as in [70]), a weak *trajectory-only* 2D projection guidance can be used at inference to nudge projected end-effector paths toward \mathbf{T}_{2D} when sketches are reliable. We use classifier-free guidance with 10% conditional dropout during training and guidance weight $\omega \in [1.4, 1.8]$ at inference.

3.2. Dual-Space Conditioning

Sketch constraints are inherently sparse, touching only a subset of joints, frames, and anchors. A fundamental challenge arises: enforcing constraints purely in raw motion space can satisfy visible constraints while drifting off-manifold elsewhere, whereas enforcing them purely in latent space preserves stylistic coherence but sacrifices precise geometric accuracy. We therefore introduce a dual-space conditioning mechanism that synergistically combines raw-space precision with latent-space consistency. Our approach operates through two tightly coupled pathways. First, we define differentiable energies on decoded motions $\Pi(\mathbf{z}) = \mathcal{D}(\mathbf{z})$ (detailed in Section 3.3) and efficiently back-propagate their gradients to latent space using a learned low-rank, block-Toeplitz Jacobian surrogate $\mathbf{B}_\rho \approx (\partial\mathcal{D}/\partial\mathbf{z})^\top$. This yields a raw-space guidance vector:

$$\mathbf{g}_{\text{raw}}(\mathbf{z}) = \mathbf{B}_\rho \nabla_{\mathbf{M}_{1:N}} \left(\sum_r \lambda_r E_r(\Pi(\mathbf{z})) \right) \in \mathbb{R}^{T_{\text{lat}} \times V \times d} \quad (7)$$

Second, we introduce *latent anchors* that leverage our aligned 2D \leftrightarrow 3D encoders from Eq. (2). For each condition type $y \in \{k, \tau, o\}$, we form target embeddings $\mathbf{s}_y^* = \mathcal{E}_y^{3D}(\hat{\mathbf{M}}_{1:N})$ where $\hat{\mathbf{M}}_{1:N}$ denotes only the constrained subset specified by \mathcal{X} . A lightweight projection head $f_\gamma : \mathbb{R}^{T_{\text{lat}} \times V \times d} \rightarrow \mathbb{R}^{d_e}$ maps the current latent to this embedding space, and we enforce agreement via $\mathcal{L}_{\text{lat}} = \sum_y \|f_\gamma(\mathbf{z}) - \text{sg}[\mathbf{s}_y^*]\|_2^2 + \lambda_{\text{NCE}} \mathcal{L}_{\text{InfoNCE}}$, where $\text{sg}[\cdot]$ denotes stop-gradient for encoder.

This provides us with raw-space energies that can provide fine precision for contacts and trajectories, while latent anchors suppress off-manifold solutions by maintaining proximity to the COLLAGE prior’s learned distribution. During training, we integrate both signals by adding latent agreement to the teacher’s conditioning path and injecting $-\eta_{\text{lat}} \nabla_{\mathbf{z}} \mathcal{L}_{\text{lat}}$ as an auxiliary conservative field into the student’s velocity. This design is similar to CLIP[49, 70],

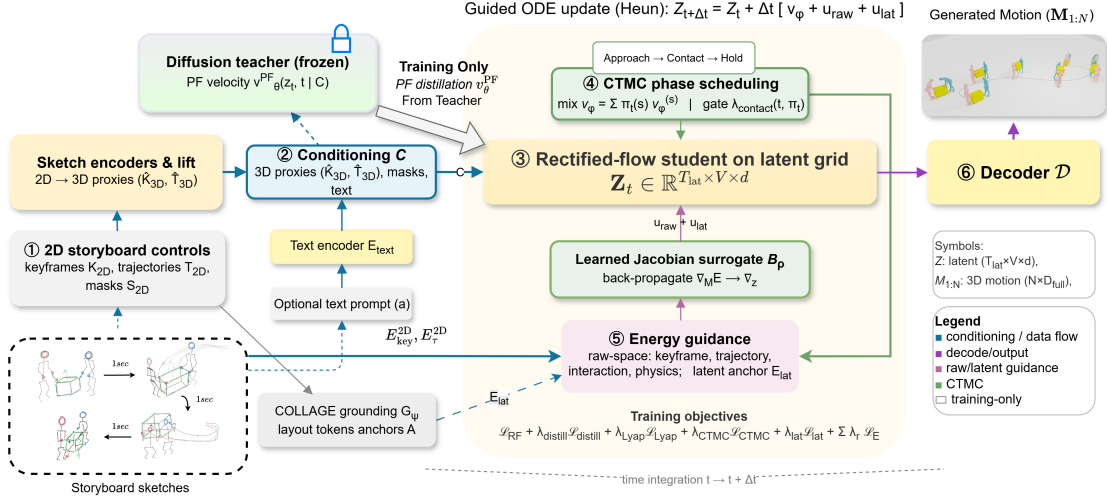


Figure 2. **Architecture of Sketch2Colab: storyboard → 3D HOH motion (1–6).** ① The user provides sketches (keyframes, per-joint 2D paths, object masks) and an optional text prompt; ② paired 2D/3D encoders produce aligned embeddings and 3D proxies, which are fused into C ; ③ a PF-distilled rectified-flow student $v_\phi(z, t | C)$ evolves latents under a frozen teacher; ④ a CTMC over phases modulates sub-fields and contact weights via π_t ; ⑤ raw-space energies and latent anchors define dual-space guidance, implemented through a learned Jacobian surrogate and applied as u_{raw} and u_{lat} in the ODE update; ⑥ a frozen decoder \mathcal{D} yields the final motion, optimized with a combination of RF, distillation, Lyapunov, CTMC, latent, and energy losses (Secs. §3.1–§3.4).

adapted here to preserve motion-specific geometric and temporal constraints.

3.3. Energy Guidance and Objective

While latent anchors maintain global coherence, precise satisfaction of sparse sketch constraints requires explicit energy formulations that can navigate the complex landscape of multi-entity interactions. We now detail how storyboard inputs translate into differentiable energies and how these energies guide the rectified flow toward feasible solutions.

To steer the student toward feasibility, we define task-specific energies on decoded motion and a Lyapunov-like potential that cooperates with them. Let $\Pi(z) = \mathcal{D}(z)$ be the decoded sequence and $\mathbf{p}_{t,j}^{(h)} \in \mathbb{R}^3$ the world-space joint of human h (projected when needed as $\tilde{\mathbf{p}}_{t,j}^{(h)} = \Pi_{\text{cam}}(\mathbf{p}_{t,j}^{(h)})$). From storyboard inputs we obtain lightweight 3D proxies ($\hat{\mathbf{K}}_{3D}, \hat{\mathbf{T}}_{3D}$) via the aligned 2D→3D encoders (Sec. 3.1, Eq. (2)). We combine 3D-proxy terms—which provide robust, low-variance targets handling depth ambiguity and sketch noise—with time-gated 2D terms that preserve visible fidelity in the storyboard plane. To keep the 2D supervision both local and robust, we use small gates in $[0, 1]$: a keyframe time gate $g_{\text{time}}(t)$ that localizes 2D keypose penalties around the annotated times \mathcal{T}_{key} , a per-joint quality score $g_{\text{qual}}(t, h, j)$ that softly down-weights noisy or lift-inconsistent strokes, and for trajectories a path gate $g_{\text{path}}(t; \mathbf{T}_{2D}^{(h,j)})$ that activates the path only on the storyboard interval associated with that stroke. We parametrize the effective 2D weights as $\lambda_{\text{key}}^{2D}(t, h, j) = \bar{\lambda}_{\text{key}}^{2D} g_{\text{time}}(t) g_{\text{qual}}(t, h, j)$ and $\lambda_{\tau}^{2D}(t, h, j) = \bar{\lambda}_{\tau}^{2D} g_{\text{path}}(t; \mathbf{T}_{2D}^{(h,j)}) g_{\text{qual},\tau}(t, h, j)$, so each energy term still acts per-frame but with a strength that depends on the current time and sketch quality.

For keyframe alignment, $E_{\text{key}}(z)$ is calculated as, $E_{\text{key}}^{3D} + E_{\text{key}}^{2D}$ with E_{key}^{3D} being $\lambda_{\text{key}}^{3D} \sum_{t \in \mathcal{T}_{\text{key}}} \sum_{h,j} \chi_{t,h,j} \|\mathbf{p}_{t,j}^{(h)} - \hat{\mathbf{K}}_{3D}[t, j]\|_2^2$ and E_{key}^{2D} being $\sum_{t \in \mathcal{T}_{\text{key}}} \sum_{h,j} \lambda_{\text{key}}^{2D}(t, h, j) \chi_{t,h,j} \|\tilde{\mathbf{p}}_{t,j}^{(h)} - \hat{\mathbf{K}}_{2D}[t, j]\|_2^2$.

Similarly for trajectories, $E_{\tau}(z)$ is calculated as, $E_{\tau}^{3D} + E_{\tau}^{2D}$ with E_{τ}^{3D} being $\lambda_{\tau}^{3D} \sum_{t,h,j} \chi_{t,h,j} \text{dist}(\mathbf{p}_{t,j}^{(h)}, \hat{\mathbf{T}}_{3D}^{(h,j)})^2$ and E_{τ}^{2D} being $\sum_{t,h,j} \lambda_{\tau}^{2D}(t, h, j) \chi_{t,h,j} \text{dist}(\tilde{\mathbf{p}}_{t,j}^{(h)}, \mathbf{T}_{2D}^{(h,j)})^2$, here $\text{dist}(\cdot, \cdot)$ is a soft closest-point distance. Interaction energies cover contact and spacing: for any designated contact pair (u, v) (e.g., left hand of h and anchor ℓ of object o), we penalize the deviation of signed distances from a target margin, $E_{\text{int}} = \sum_{t,(u,v)} \psi_{\delta}(d(\mathbf{x}_{t,u}, \mathbf{x}_{t,v}))$ with Huber penalty ψ_{δ} and distance $d(\cdot, \cdot)$ in either world space or along object surface SDFs; additional spacing terms discourage interpenetrations and enforce bimanual symmetry for paired actions. Finally, physics energies include foot-skating suppression via near-zero horizontal velocity during stance phases (detected from vertical GRF proxies), ground-plane constraints, and Laplacian smoothness along time for both pose and root translation. We schedule the contribution of each term by time-dependent weights $\lambda_r(t)$, prioritizing keyframe hits early, tightening interaction margins mid-trajectory, and enforcing physics late, which helps avoid oscillatory behavior that can arise when all objectives compete uniformly from the start.

In addition to these raw-space energies, we reuse the latent anchor from Sec. 3.2 as an explicit latent-space energy. Concretely, we define, $E_{\text{lat}}(z) = \sum_{y \in \{k, \tau, o\}} \|f_{\gamma}(z) - \mathbf{s}_y^{2D}\|_2^2 + \lambda_{\text{NCE}} \text{InfoNCE}$, here f_{γ} maps the current latent z into the shared embedding

space and s_y^{2D} are frozen storyboard embeddings from the 2D encoders corresponding to keyposes, trajectories, and objects. This term encourages the latent to stay close to the sketch-conditioned manifold while the raw-space energies refine precise geometry and contacts. During training, its supervised counterpart \mathcal{L}_{lat} from Sec. 3.2 is optimized jointly with the other losses (see Eq. (10)); at inference, E_{lat} is simply treated as another energy E_r inside the total potential.

Beyond these hand-designed energies, we learn a potential $V_\psi(\mathbf{z})$ that captures residual preferences of the motion manifold not expressed by explicit terms. The potential is trained by energy-equilibrium matching [6] with two phases: an optimal-transport warm-up in which we learn to assign lower potential to teacher samples than to latent noise, and a contrastive divergence refinement in which short Langevin chains on \mathbf{z} define negative examples. The student is then trained to produce velocities that are descending directions of the total potential $\mathcal{V}(\mathbf{z}, t) = V_\psi(\mathbf{z}) + \sum_r \lambda_r(t) E_r(\mathbf{z}) + \lambda_{\text{lat}} E_{\text{lat}}(\mathbf{z})$ by minimizing,

$$\mathcal{L}_{\text{Lyap}}(\phi, \psi) = \mathbb{E}_t \left[\left(\max\{0, \nabla_{\mathbf{z}} \mathcal{V}(\mathbf{z}, t) \cdot v_\phi(\mathbf{z}, t) + \kappa \|\nabla_{\mathbf{z}} \mathcal{V}(\mathbf{z}, t)\|_2^2 \} \right)^2 \right] \quad (8)$$

with small $\kappa > 0$ acting as a margin; gradients $\nabla_{\mathbf{z}} E_r$ and $\nabla_{\mathbf{z}} E_{\text{lat}}$ are computed via the surrogate \mathbf{B}_ρ as discussed above. Practically, we treat $-\nabla_{\mathbf{z}} \mathcal{V}$ as an additional, conservative guidance vector added to the student’s velocity during both training and inference, which yields a stable, monotone approach to constraint satisfaction while keeping the flow close to the sketch-conditioned latent manifold.

3.4. Discrete Phase Scheduling via CTMC

Now, a distinctive feature of everyday interactions is that they involve switching between discrete phases (approach, contact, hold/handover), which continuous fields tend to smear in time. We model phase occupancy with a CTMC[28] and mix sub-velocities accordingly. To enable seamless transition across such changes of state we therefore couple a continuous-time Markov chain (CTMC) over interaction states $s \in \{1, \dots, S\}$ with occupancy $\pi_t \in \Delta^{S-1}$ to the flow. Transition rates are given by a locally equivariant MLP $Q_\eta(\mathbf{h}_t) \in \mathbb{R}^{S \times S}$ with nonnegative off-diagonals and row sums zero, where \mathbf{h}_t are per-time features extracted from the latent (pooled over relevant entity tokens) together with distances to designated anchors; the Kolmogorov forward equation[28] $d\pi_t/dt = \pi_t Q_\eta(\mathbf{h}_t)$ is enforced by the loss

$$\mathcal{L}_{\text{CTMC}}(\eta) = \mathbb{E}_t \left\| \frac{d\pi_t}{dt} - \pi_t Q_\eta(\mathbf{h}_t) \right\|_2^2 + \beta \text{Var}[A_t(Q_\eta)], \quad (9)$$

where A_t denotes an optional entropy-like regularizer on the rate spectrum. The CTMC modulates the student in two ways that preserve the backbone: (i) we form a convex mixture of phase-specific sub-fields, $v_\phi(\mathbf{z}, t) = \sum_{s=1}^S \pi_t(s) v_\phi^{(s)}(\mathbf{z}, t)$ and (ii) we scale contact energies in \mathcal{V} by the expected contact occupancy, keeping contact terms quiescent pre-grasp and strong post-grasp. For

a two-keyframe sketch with $t_1=0.3$ (near-contact) and $t_2=0.7$ (grasped), the chain maintains $\pi_t(\text{contact}) \approx 0$ before t_1 (smooth approach); near t_2 mass shifts to the contact state, increasing contact gains and activating a grasp-specialized sub-field, yielding crisp, non-oscillatory phase transitions.

With the teacher frozen, the student (and auxiliary modules ψ, η) are trained with the combined objective,

$$\mathcal{L} = \mathcal{L}_{\text{RF}} + \lambda_{\text{dist}} \mathcal{L}_{\text{distill}} + \lambda_{\text{Lyap}} \mathcal{L}_{\text{Lyap}} + \sum_r \lambda_r \mathcal{L}_{E_r} + \lambda_{\text{lat}} \mathcal{L}_{\text{lat}} + \lambda_{\text{CTMC}} \mathcal{L}_{\text{CTMC}} + \lambda_{\text{cons}} \mathcal{L}_{\text{consist}}, \quad (10)$$

where \mathcal{L}_{E_r} are supervised surrogates for energy terms with ground truth (e.g., binary contact labels), and $\mathcal{L}_{\text{consist}}$ enforces segment-overlap consistency for long clips per [17].

4. Experimental Setup

We now evaluate *Sketch2Colab* on multi-entity HOH scenarios. Our experiments are designed to answer three questions: (i) can the model faithfully follow storyboard keyposes and joint/object trajectories, (ii) does it improve interaction quality (contacts, collisions, spacing) over sketch-driven baselines, and (iii) how does the rectified-flow + CTMC design compare to diffusion-only alternatives in terms of alignment and sampling cost. Below we summarize the datasets, storyboard synthesis, training/inference setup, and evaluation metrics; additional details are provided in the *Supp. Sec. 4*.

Datasets and storyboard synthesis. We train and evaluate on **CORE4D** [67] and **InterHuman** [40]. CORE4D provides 998 multi-human, object-centric interaction sequences; we follow an 80/5/15 train/val/test split as in [17]. For InterHuman, we use all 6,022 multi-human sequences with the same split, which further enriches interaction diversity. For each 3D motion clip, we synthesize storyboard controls by projecting 3D joints onto the sketch plane and rasterizing per-joint 2D polylines with perturbations (jitter, small contour noise) to mimic hand-drawn strokes, building on SKETCH2ANIM [70] and also utilise set of 682 hand-drawn sketches over CORE4D sequences. We use the same camera setup as SKETCH2ANIM [70] and annotate K keyframes per clip at motion-salient times (contacts, reversals, phase changes for optional text conditioning), yielding 2D keyposes \mathbf{K}_{2D} and 2D joint paths \mathbf{T}_{2D} as described in Sec. 3.

Teacher-student training and inference. *Sketch2Colab* distills a *COLLAGE* diffusion teacher into a rectified-flow student operating in the same latent space (Sec. 3). We first train the teacher with AdamW for 400k steps (learning rate 2×10^{-4} , batch size 64, EMA 0.999, weight decay 0.01) using 1000 diffusion steps [27], then freeze the teacher and distill its probability-flow field into the student. The student is trained for 500k steps with learning

Table 1. **CORE4D: baselines and ablations (Average protocol)**. R-Precision(Higher is better); lower is better otherwise. Control accuracy follows [70] with Keypose/Trajectory in 2D and 3D. Cross-protocol[70] results and InterHuman[40] Metric comparison are provided in the supplementary (Supp. Sec. S.5).

Method	Realism		Control Accuracy				Interaction			Text-Motion	
	FID ↓	Foot-skate ↓	Key-2D ↓	Key-3D ↓	Traj-2D ↓	Traj-3D ↓	ObjPos-3D ↓	Anchor-Err ↓	Penetration ↓	MM Dist ↓	R-Prec (Top-3) ↑
<i>Baselines (HOH setting)</i>											
Retrieval-INT	0.700	0.080	0.0570	0.0760	0.290	0.410	0.093	0.088	0.022	6.786	0.426
Sketch2Anim-INT (adapted)	0.880	0.132	0.0590	0.0790	0.154	0.251	0.071	0.102	0.048	6.822	0.435
COLLAGE Teacher (base)	0.620	0.125	0.0520	0.0690	0.121	0.219	0.058	0.082	0.032	6.529	0.453
Sketch2Colab (ours)	0.480	0.095	0.0360	0.0478	0.0867	0.134	0.041	0.045	0.025	6.040	0.471
<i>Ablations (Sketch2Colab variants)</i>											
Sketch2Colab w/o Energy	0.563	0.111	0.0397	0.0532	0.111	0.171	0.051	0.089	0.029	6.155	0.465
Sketch2Colab w/o CTMC	0.518	0.111	0.0381	0.0509	0.0951	0.151	0.048	0.059	0.030	6.081	0.467
Sketch2Colab w/o Collage grounding	0.507	0.099	0.0370	0.0495	0.0890	0.143	0.051	0.055	0.028	6.074	0.470
Sketch2Colab w/o Temporal bias	0.497	0.099	0.0369	0.0487	0.0920	0.140	0.043	0.051	0.025	6.063	0.469
Sketch2Colab Parallel ControlNets	0.528	0.104	0.0384	0.0503	0.101	0.147	0.048	0.056	0.026	6.095	0.468
Sketch2Colab Trajectory-only route	0.579	0.109	0.0418	0.0553	0.116	0.171	0.053	0.071	0.027	6.178	0.463
Sketch2Colab (full)	0.480	0.095	0.0360	0.0478	0.0867	0.134	0.041	0.045	0.025	6.040	0.471

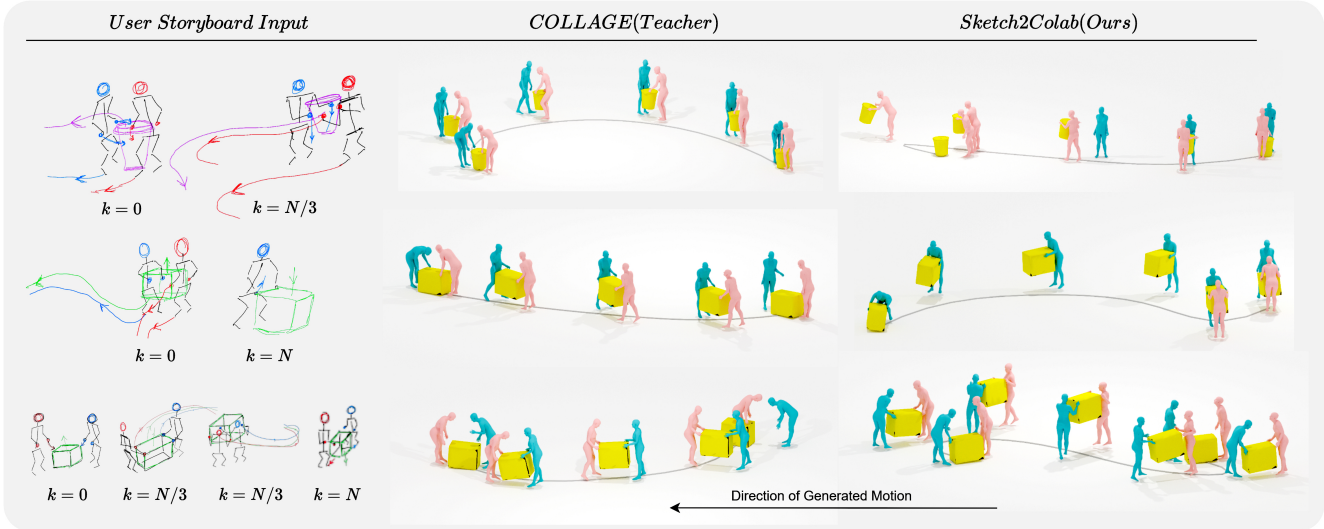


Figure 3. **Sketch→interaction motion: comparison of Sketch2Colab and COLLAGE (teacher)** [17]. Given storyboard keyframes and joint trajectories (top), *Sketch2Colab* (right) generates HOH motions that closely follow the sketches, execute interaction phases at the intended times, and adhere tightly to trajectories and keyframes. In contrast, COLLAGE (teacher, middle) struggles to respect storyboard constraints such as the handover and continued motion with a single human holding the object(1st and 2nd storyboards), and fails to match fine-grained keyframe constraints (e.g., the third storyboards, where the character must lift higher while moving). Additional examples and baseline comparisons are provided in the *Supp. Sec. S.5*

Table 2. Storyboard (sketch-only unless specified) HOH on CORE4D[67]. Noise levels $\approx 60\%$ correspond to Fig. 4C.

Method / Condition	Noise	FID↓	Foot↓	Traj↓	Anch↓	Pen↓	R-Prec↑
<i>(a) Method Comparison & Ablations (Sketch-only)</i>							
SKETCH2ANIM-INT (adapted)	—	1.025	0.154	0.292	0.119	0.056	0.363
COLLAGE[17] teacher	—	0.735	0.148	0.260	0.097	0.038	0.369
Sketch2Colab	—	0.509	0.098	0.139	0.046	0.025	0.437
w/o CTMC	—	0.548	0.114	0.158	0.061	0.031	0.428
w/o Energy	—	0.597	0.118	0.182	0.094	0.031	0.421
<i>(b) Sketch-only Noise Robustness</i>							
Sketch2Colab	20%	0.551	0.119	0.178	0.067	0.034	0.396
	40%	0.598	0.126	0.214	0.091	0.041	0.374
	60%	0.729	0.151	0.287	0.134	0.052	0.331
	80%	0.894	0.172	0.381	0.186	0.071	0.278
<i>(c) Sketch+Text Noise Robustness</i>							
Sketch2Colab	0%	0.480	0.095	0.134	0.045	0.025	0.471
	20%	0.498	0.102	0.153	0.054	0.026	0.467
	40%	0.543	0.111	0.188	0.076	0.033	0.458
	60%	0.657	0.132	0.247	0.112	0.039	0.442
	80%	0.782	0.144	0.322	0.149	0.057	0.419

rate 10^{-4} and batch size 64. In the first phase we minimize $\mathcal{L}_{RF} + \lambda_{\text{dist}}\mathcal{L}_{\text{distill}}$ only, to match the teacher’s transport field; in the second phase we activate the Lyapunov and CTMC losses and the supervised energy surrogates, optimizing the

full objective in Eq. (10). Unless otherwise stated we set $\lambda_{\text{dist}}=0.5$, $\lambda_{\text{Lyap}}=0.5$, $\lambda_{\text{CTMC}}=0.1$, $\lambda_{\text{lat}}=0.1$, and anneal the energy weights $\lambda_r(t)$ according to the early/mid/late schedule described in Sec. 3.3. At inference time, we draw $\mathbf{z}_1 \sim \mathcal{N}(0, \mathbf{I})$ and, conditioning on the storyboard controls \mathcal{C} , integrate the guided ODE for $T_{\text{int}} \in [30, 60]$ Heun steps (we use $T_{\text{int}}=30$ on CORE4D and $T_{\text{int}}=60$ on InterHuman), interleaving CTMC updates every $s=3$ steps and using classifier-free guidance weight $\omega \in [1.4, 1.8]$ (default $\omega=1.6$). After the ODE pass, we *optionally* apply a short micro-Langevin refinement in latent space: $K_{\text{corr}}=3$ Langevin steps with step size $\eta_{\text{corr}}=1 \times 10^{-3}$ using the teacher score, which slightly sharpens high-frequency details and improves constraint satisfaction without altering global motion. The final 3D motion $\mathbf{M}_{1:N}$ is obtained by decoding the last latent state \mathbf{z}_0 with the COLLAGE decoder. The student architecture follows the temporal U-Net design of COLLAGE [17].

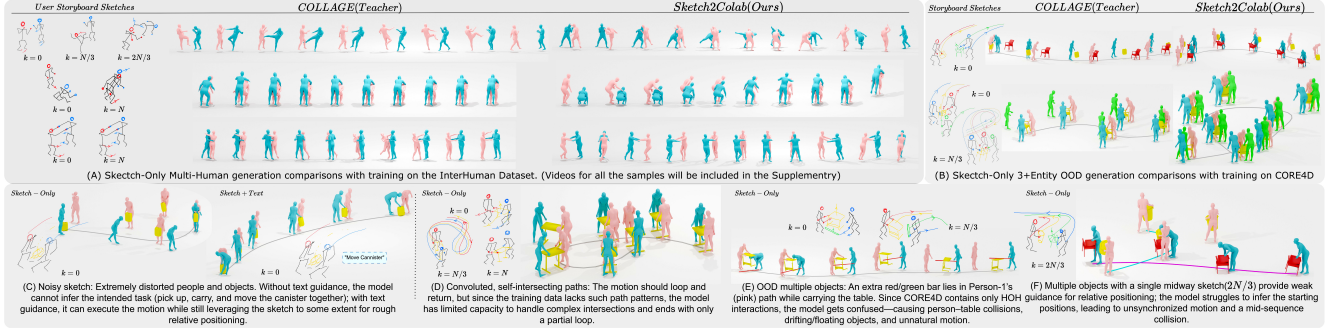


Figure 4. **Qualitative motion frames, trajectories, and limitations.** (A,B) Sketch-only comparisons to Collage teacher on InterHuman[40] (HH) and CORE4D[67] (3+ entity OOD). (C–F) Hard cases: heavy sketch noise ($\approx 60\%$, Tab.2 (b,c)), self-intersecting paths, and OOD multi-object / sparse-constraints causing drift, floating, or collisions.

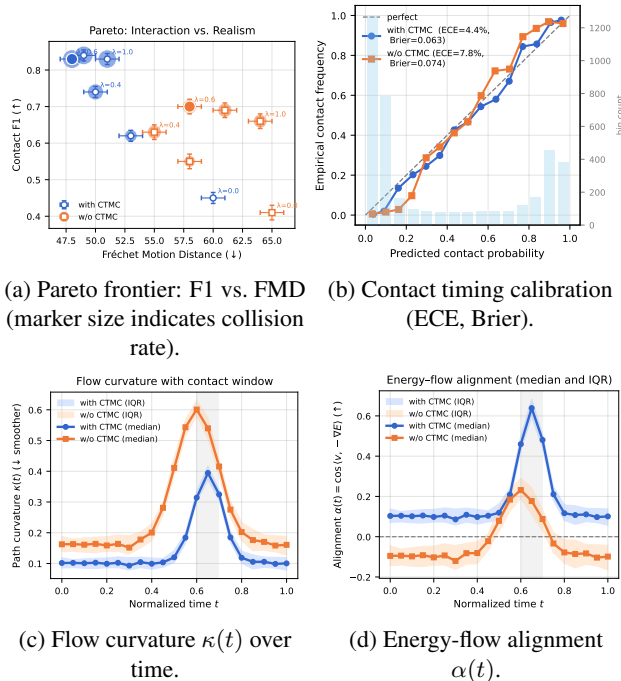


Figure 5. **Impact of CTMC and energy guidance.** (a) CTMC shifts the F1–FMD Pareto frontier outward while reducing collision rates. (b) Contact timing calibration improves significantly (lower ECE). (c) Flow maintains low curvature except at discrete mode transitions. (d) Energy gradient aligns constructively with base flow near transitions, eliminating gradient conflicts.

Metrics. We report realism (FID, Foot-skate), control accuracy (Keypose-2D/3D, Trajectory-2D/3D under the *Average* protocol [70]), interaction quality (ObjPos-3D, Anchor-Err, Penetration), and text–motion alignment (MM Dist, R-Precision Top-3 [17, 56, 70]). (Full definitions and implementation details are provided in the Supp. Sec. S.4)

5. Results and Analysis

Overview. Table 1 reports comparisons across realism, control accuracy, interaction quality, and text–motion alignment on CORE4D. *Sketch2Colab* establishes a stronger operating point across all categories critical for storyboard-driven HOH: it reduces realism errors, tightens both

keyframe and trajectory adherence in 2D and 3D, materially improves object/anchor interaction while suppressing penetrations, and strengthens text–motion alignment. We see similar results over InterHuman dataset (Supp. Sec. S.5).

Relative to the *COLLAGE* teacher, *Sketch2Colab* cuts FID by roughly **23%** and foot-skate by about **24%**. Control accuracy improves across all channels: Key-2D/3D errors drop by around **31%**, Traj-2D by **28%**, and Traj-3D by almost **40%**. On HOH interaction, *Sketch2Colab* reduces object-position error by nearly **30%**, anchor error by about **45%**, and penetration by about **22%**, yielding crisper keyframe hits, better path following, and much cleaner contacts than a diffusion-only backbone. Despite being primarily sketch-controlled compared to LLM based planning in *COLLAGE*[17], it also improves text–motion alignment, with MM Dist decreasing by about **7%** and R-Precision (Top-3) increasing by roughly **4%**.

Comparison to adapted baselines. Against the adapted diffusion baseline *Sketch2Anim-INT*, *Sketch2Colab* achieves markedly better realism and interaction: it reduces FID and Traj-3D by **45–50%**, anchor errors by more than **50%**, and penetration errors by about **48%**, while also tightening keyframe control. These improvements stem from operating in a structured latent space with energy-guided rectified flows rather than raw motion space alone. Retrieval-based matching records the smallest absolute foot-skate and penetration instances, as expected from reusing database motion, and benefits from *COLLAGE*-style text retrieval cues, but it lags substantially on control and specified interaction and cannot realize novel compositions. In contrast, *Sketch2Colab* combines near-retrieval smoothness with significantly higher fidelity to sketch constraints and interaction intent.

Ablations. The ablation block in Table 1 isolates specific aspects of *Sketch2Colab*’s design. Removing *energy guidance* produces the largest drop in performance: realism and stance worsen by around **15–20%**, trajectory and object-position errors increase by roughly **25–30%**, anchor error roughly doubles, and penetration increases by about **16%**,

confirming that conservative energy descent is the primary driver of safe, precise contacts. Disabling *CTMC scheduling* mainly harms temporal phasing—foot-skate and trajectory errors rise by roughly **10–20%**, with anchor errors up by around **30%** and penetration by about **20%**—which matches its role in staging approach, contact, and hold. Removing *collage grounding* leads to moderate but focused regressions in layout: object and anchor errors increase by about **20–25%** and penetration by roughly **12%**, while global control remains relatively stable. Ablating the *temporal phase bias* yields smaller yet systematic drops (typically single-digit to low double-digit percentages) concentrated on mid-sequence trajectories and contact timing, consistent with a soft timing prior. Replacing the unified adapters with *Parallel ControlNets* causes broad but moderate degradation—on the order of **10–25%** across realism, control, and interaction—indicating that decoupled control branches make guidance compete rather than cooperate. Finally, a *trajectory-only* route erodes both control and interaction most severely: keyframe and trajectory errors grow by roughly **15–35%**, object and anchor errors by around **30–60%**, and penetration by about **8%**, underscoring the necessity of combining keyframe snaps and latent anchors with trajectory shaping for fine-grained, contact-aware control. Additional ablations and evaluations are provided in the *Supp. Sec. S.5*.

Qualitative Analysis. The qualitative panels in Figure 3 and in the Supplementary mirror the table trends: *Sketch2Colab* follows sketched paths tightly, aligns closely with suggested anchor points, and generates poses that closely resemble the storyboard controls. The model executes phase transitions between keyframes at the intended times and maintains crisp object alignment and interaction without accumulating spurious motion. In contrast, adapted baselines drift, over-constrain prematurely/or not at all, or transition to unintended motions or interactions. We observe hanging objects and dis-coordinated interactions across all motions except those produced by *Sketch2Colab*; retrieval-based generation provides smooth motion but with noticeably weaker constraint adherence.

6. Discussion and Future Work

We introduced *Sketch2Colab*, a storyboard-driven rectified-flow framework with CTMC phase scheduling, dual-space guidance, and latent anchors that together yield strong realism, control accuracy, and interaction quality for HOH generation, while retaining efficient sampling. Our model still has limitations: object handling and collaboration are learned on the object categories present in CORE4D, the setting focuses on one-to-one hand-object interaction rather than multi-human coordination, and the flow-based student relies on a calibrated diffusion teacher. In future work, we aim to support arbitrary objects given a mesh and physical properties, extend to multi-human interaction via compo-

sitional field models without requiring 2+ human datasets, and explore training strategies that weaken or remove the dependence on a diffusion prior.

References

- [1] Kfir Aberman, Yijia Weng, Dani Lischinski, Daniel Cohen-Or, and Baoquan Chen. Unpaired motion style transfer from video to animation. *ACM Transactions on Graphics (TOG)*, 39(4):64–1, 2020. 1, 2
- [2] Michael Albergo and Eric Vanden-Eijnden. Building normalizing flows with stochastic interpolants. In *International Conference on Learning Representations (ICLR)*, 2023. 2
- [3] Nikos Athanasiou, Mathis Petrovich, Michael J Black, and Gül Varol. Teach: Temporal action composition for 3d humans. In *2022 International Conference on 3D Vision (3DV)*, pages 414–423. IEEE, 2022. 2
- [4] Nikos Athanasiou, Alpár Cseke, Markos Diomataris, Michael J. Black, and Gül Varol. Motionfix: Text-driven 3d human motion editing. In *SIGGRAPH Asia 2024 Conference Papers*, 2024. 1, 2
- [5] Shaojie Bai, J. Z. Kolter, and V. Koltun. An empirical evaluation of generic convolutional and recurrent networks for sequence modeling. *arXiv*, 2018. 4
- [6] Michal Balcerak, Tamaz Amiranashvili, Antonio Terpin, Suprosanna Shit, Lea Bogensperger, Sebastian Kaltenbach, Petros Koumoutsakos, and Bjoern Menze. Energy matching: Unifying flow matching and energy-based models for generative modeling. *arXiv preprint arXiv:2504.10612*, 2025. 2, 3, 6
- [7] G Barquero, S Escalera, and C Palmero. BeLFusion: Latent diffusion for behavior-driven human motion prediction. In *ICCV*, 2023. 2
- [8] Heli Ben-Hamu, Omri Puny, Itai Gat, Brian Karrer, Uriel Singer, and Yaron Lipman. D-flow: differentiating through flows for controlled generation. In *International Conference on Machine Learning (ICML)*, 2024. 2, 3
- [9] Mikhail Bessmeltsev, Nicholas Vining, and Alla Sheffer. Gesture3d: posing 3d characters via gesture drawings. *ACM Transactions on Graphics (TOG)*, 2016. 3
- [10] Kirill Brodt and Mikhail Bessmeltsev. Sketch2pose: estimating a 3d character pose from a bitmap sketch. *ACM Transactions on Graphics (TOG)*, 2022. 3
- [11] Ling-Hao Chen, Jiawei Zhang, Yewen Li, Yiren Pang, Xi-aobo Xia, and Tongliang Liu. HumanMAC: Masked motion completion for human motion prediction. In *ICCV*, 2023. 2
- [12] Ling-Hao Chen, Wenxun Dai, Xuan Ju, Shunlin Lu, and Lei Zhang. Motionclr: Motion generation and training-free editing via understanding attention mechanisms. *arXiv preprint arXiv:2410.18977*, 2024. 1, 2
- [13] Xin Chen, Biao Jiang, Wen Liu, Zilong Huang, Bin Fu, Tao Chen, and Gang Yu. Executing your commands via motion diffusion in latent space. In *Proceedings of the IEEE/CVF Conference on Computer Vision and Pattern Recognition*, 2023. 2, 3
- [14] Hyungjin Chung, Jeongsol Kim, Michael T Mccann, Marc L Klasky, and Jong Chul Ye. Diffusion posterior sam-

- pling for general noisy inverse problems. *arXiv preprint arXiv:2209.14687*, 2022. 2, 3
- [15] Setareh Cohan, Guy Tevet, Daniele Reda, Xue Bin Peng, and Michiel van de Panne. Flexible motion in-betweening with diffusion models. In *ACM SIGGRAPH 2024 Conference Papers*, 2024. 1, 2
- [16] Peishan Cong, Ziyi Wang, Zhiyang Dou, Yiming Ren, Wei Yin, Kai Cheng, Yujing Sun, Xiaoxiao Long, Xinge Zhu, and Yuexin Ma. LaserHuman: Language-guided scene-aware human motion generation in free environment. *arXiv*, 2024. 1, 2
- [17] Divyanshu Daiya, Damon Conover, and Aniket Bera. Collage: Collaborative human-agent interaction generation using hierarchical latent diffusion and language models. In *2025 IEEE International Conference on Robotics and Automation (ICRA)*, pages 8203–8210. IEEE, 2025. 1, 2, 3, 4, 6, 7, 8
- [18] Prafulla Dhariwal and Alexander Nichol. Diffusion models beat gans on image synthesis. *Advances in neural information processing systems*, 34:8780–8794, 2021. 2
- [19] Yilun Du and Igor Mordatch. Implicit generation and generalization in energy-based models. In *Advances in Neural Information Processing Systems (NeurIPS)*, 2019. 2, 3
- [20] Patrick Esser, Sumith Kulal, Andreas Blattmann, Rahim Entezari, Jonas Müller, Harry Saini, Yam Levi, Dominik Lorenz, Axel Sauer, Frederic Boesel, et al. Scaling rectified flow transformers for high-resolution image synthesis. In *Forty-first International Conference on Machine Learning*, 2024. 2, 3
- [21] Anindita Ghosh, Rishabh Dabral, Vladislav Golyanik, Christian Theobalt, and Philipp Slusallek. ReMoS: Reactive 3d motion synthesis for two-person interactions. *arXiv*, 2023. 1, 2
- [22] Martin Guay, Rémi Ronfard, Michael Gleicher, and Marie-Paule Cani. Space-time sketching of character animation. *ACM Transactions on Graphics (ToG)*, 2015. 3
- [23] Chuan Guo, Xinxin Zuo, Sen Wang, Shihao Zou, Qingyao Sun, Annan Deng, Minglun Gong, and Li Cheng. Action2motion: Conditioned generation of 3d human motions. In *Proceedings of the 28th ACM International Conference on Multimedia*, pages 2021–2029, 2020. 2
- [24] Chuan Guo, S. Zou, X. Zuo, S. Wang, W. Ji, X. Li, and L. Cheng. Generating diverse and natural 3d human motions from text. In *CVPR*, 2022. 1
- [25] Ziyang Guo, Zeyu Hu, De Wen Soh, and Na Zhao. Motionlab: Unified human motion generation and editing via the motion-condition-motion paradigm. In *Proceedings of the IEEE/CVF International Conference on Computer Vision*, pages 13869–13879, 2025. 2, 3
- [26] Fabian Hahn, Frederik Mutzel, Stelian Coros, Bernhard Thomaszewski, Maurizio Nitti, Markus Gross, and Robert W. Sumner. Sketch abstractions for character posing. In *Proceedings of the 14th ACM SIGGRAPH/Eurographics Symposium on Computer Animation*, pages 185–191, 2015. 3
- [27] Jonathan Ho, Ajay Jain, and Pieter Abbeel. Denoising diffusion probabilistic models. In *Advances in Neural Information Processing Systems (NeurIPS)*, 2020. 2, 4, 6
- [28] Peter Holdrieth, Marton Havasi, Jason Yim, Neta Shaul, Itai Gat, Tommi Jaakkola, Brian Karrer, Ricky TQ Chen, and Yaron Lipman. Generator matching: Generative modeling with arbitrary markov processes. *arXiv preprint arXiv:2410.20587*, 2024. 2, 3, 6
- [29] Siyuan Huang, Zan Wang, Puhao Li, Baoxiong Jia, Tengyu Liu, Yixin Zhu, Wei Liang, and Song-Chun Zhu. Diffusion-based generation, optimization, and planning in 3d scenes. In *CVPR*, 2023. 1, 2
- [30] Wenlong Huang, P. Abbeel, D. Pathak, and I. Mordatch. Language models as zero-shot planners: Extracting actionable knowledge for embodied agents. In *ICML*, 2022. 3
- [31] Takeo Igarashi, Rieko Kadobayashi, Kenji Mase, and Hidehiko Tanaka. Path drawing for 3d walkthrough. In *Proceedings of the 11th annual ACM symposium on User interface software and technology*, 1998. 3
- [32] Biao Jiang, Xin Chen, Wen Liu, Jingyi Yu, Gang Yu, and Tao Chen. MotionGPT: Human motion as a foreign language. In *NeurIPS*, 2023. 1, 2, 3
- [33] Nan Jiang, Zhiyuan Zhang, Hongjie Li, Xiaoxuan Ma, Zan Wang, Yixin Chen, Tengyu Liu, Yixin Zhu, and Siyuan Huang. Scaling up dynamic human-scene interaction modeling. In *CVPR*, 2024. 1, 2
- [34] K Karunratanakul, K Preechakul, S Suwajanakorn, and Siyu Tang. GMD: Controllable human motion synthesis via guided diffusion models. In *ICCV*, 2023. 1, 2
- [35] Takeshi Kojima, S. S. Gu, M. Reid, Y. Matsuo, and Y. Iwasawa. Large language models are zero-shot reasoners. In *NeurIPS*, 2022. 3
- [36] John Lasseter. Principles of traditional animation applied to 3d computer animation. In *Seminal graphics: pioneering efforts that shaped the field*, 1998. 3
- [37] Taeryung Lee, Gyeongsik Moon, and Kyoung Mu Lee. Multiact: Long-term 3d human motion generation from multiple action labels. In *AAAI*, 2023. 2
- [38] Jiaman Li, Jiajun Wu, and C. Karen Liu. Object motion guided human motion synthesis. *ACM Transactions on Graphics (TOG)*, 2023. 2
- [39] Jiaman Li, Alexander Clegg, Roozbeh Mottaghi, Jiajun Wu, Xavier Puig, and C. Karen Liu. Controllable human-object interaction synthesis. In *European Conference on Computer Vision*, 2025. 2
- [40] Han Liang, Wenqian Zhang, Wenxuan Li, Jingyi Yu, and Lan Xu. InterGen: Diffusion-based multi-human motion generation under complex interactions. *arXiv*, 2023. 3, 6, 7, 8
- [41] Juncong Lin, Takeo Igarashi, Jun Mitani, and Greg Saul. A sketching interface for sitting-pose design. In *Proceedings of the Seventh Sketch-Based Interfaces and Modeling Symposium*, 2010. 3
- [42] Yaron Lipman, Ricky TQ Chen, Heli Ben-Hamu, Maximilian Nickel, and Matt Le. Flow matching for generative modeling. *arXiv preprint arXiv:2210.02747*, 2022. 2, 3
- [43] Xingchao Liu, Chengyue Gong, and Qiang Liu. Flow straight and fast: Learning to generate and transfer data with rectified flow. *arXiv preprint arXiv:2209.03003*, 2022. 2, 3, 4

- [44] Yunze Liu, Changxi Chen, and Li Yi. Interactive humanoid: Online full-body motion reaction synthesis with social affordance canonicalization and forecasting. *arXiv*, 2023. 1, 2
- [45] Wei Mao, M. Liu, and M. Salzmann. Generating smooth pose sequences for diverse human motion prediction. In *CVPR*, 2021. 2
- [46] OpenAI. ChatGPT. <https://chat.openai.com/>, 2023. 3
- [47] Georgios Pavlakos, Vasileios Choutas, Nima Ghorbani, Timo Bolkart, Ahmed AA Osman, Dimitrios Tzionas, and Michael J Black. Expressive body capture: 3d hands, face, and body from a single image. In *Proceedings of the IEEE/CVF conference on computer vision and pattern recognition*, pages 10975–10985, 2019. 3
- [48] Mathis Petrovich, Michael J Black, and Gül Varol. Action-conditioned 3d human motion synthesis with transformer vae. In *Proceedings of the IEEE/CVF International Conference on Computer Vision*, pages 10985–10995, 2021. 2
- [49] Alec Radford, Jong Wook Kim, Chris Hallacy, Aditya Ramesh, Gabriel Goh, Sandhini Agarwal, Girish Sastry, Amanda Askell, Pamela Mishkin, Jack Clark, et al. Learning transferable visual models from natural language supervision. In *International conference on machine learning*, pages 8748–8763. PMLR, 2021. 4
- [50] D Rempe, Z Luo, Xue Bin P, Y Yuan, K Kitani, K Kreis, S Fidler, and Or Litany. Trace and pace: Controllable pedestrian animation via guided trajectory diffusion. In *CVPR*, 2023. 1, 2
- [51] J Song, C. Meng, and S. Ermon. Denoising diffusion implicit models. *arXiv*, 2020. 2
- [52] Wenfeng Song, Xingliang Jin, Shuai Li, Chenglizhao Chen, Aimin Hao, Xia Hou, Ning Li, and Hong Qin. Arbitrary motion style transfer with multi-condition motion latent diffusion model. In *Proceedings of the IEEE/CVF Conference on Computer Vision and Pattern Recognition (CVPR)*, pages 821–830, 2024. 1, 2
- [53] Yang Song and Diederik P Kingma. How to train your energy-based models. *arXiv preprint arXiv:2101.03288*, 2021. 2
- [54] Yang Song, Jascha Sohl-Dickstein, Diederik P Kingma, Abhishek Kumar, Stefano Ermon, and Ben Poole. Score-based generative modeling through stochastic differential equations. *arXiv preprint arXiv:2011.13456*, 2020. 4
- [55] Guy Tevet, Brian Gordon, Amir Hertz, Amit H Bermano, and Daniel Cohen-Or. Motionclip: Exposing human motion generation to clip space. In *European Conference on Computer Vision*, pages 358–374. Springer, 2022. 1, 2, 4
- [56] Guy Tevet, S. Raab, B. Gordon, Y. Shafir, D. Cohen-Or, and A. H. Bermano. Human motion diffusion model. *arXiv*, 2022. 8
- [57] Guy Tevet, Sigal Raab, Brian Gordon, Yoni Shafir, Daniel Cohen-or, and Amit Haim Bermano. Human motion diffusion model. In *The Eleventh International Conference on Learning Representations*, 2023. 1, 2, 3
- [58] Matthew Thorne, David Burke, and Michiel Van De Panne. Motion doodles: an interface for sketching character motion. *ACM Transactions on Graphics (TOG)*, 2004. 3
- [59] Hugo Touvron, Louis Martin, Kevin Stone, Peter Albert, Amjad Almahairi, Yasmine Babaei, Nikolay Bashlykov, Soumya Batra, Prajjwal Bhargava, Shruti Bhosale, et al. Llama 2: Open foundation and fine-tuned chat models. *arXiv*, 2023. 3
- [60] Aaron van den Oord, Yazhe Li, and Oriol Vinyals. Representation learning with contrastive predictive coding. *arXiv preprint arXiv:1807.03748*, 2018. 4
- [61] Weilin Wan, Zhiyang Dou, Taku Komura, Wenping Wang, Dinesh Jayaraman, and Lingjie Liu. Tlcontrol: Trajectory and language control for human motion synthesis. *arXiv preprint arXiv:2311.17135*, 2023. 1, 2
- [62] Zhenzhi Wang, Jingbo Wang, Dahua Lin, and Bo Dai. InterControl: Generate human motion interactions by controlling every joint. *arXiv*, 2023. 1, 2
- [63] Richard Williams. *The animator’s survival kit: a manual of methods, principles and formulas for classical, computer, games, stop motion and internet animators*. Macmillan, 2012. 3
- [64] Yiming Xie, Varun Jampani, Lei Zhong, Deqing Sun, and Huaizu Jiang. Omnicontrol: Control any joint at any time for human motion generation. *arXiv preprint arXiv:2310.08580*, 2023. 1, 2, 3, 4
- [65] Innfarn Yoo, Juraj Vanek, Maria Nizovtseva, Nicoletta Adamo-Villani, and Bedrich Benes. Sketching human character animations by composing sequences from large motion database. *The Visual Computer*, 2014. 3
- [66] Ye Yuan and K. Kitani. DLow: Diversifying latent flows for diverse human motion prediction. In *ECCV*, 2020. 2
- [67] Chengwen Zhang, Yun Liu, Ruofan Xing, Bingda Tang, and Li Yi. Core4d: A 4d human-object-human interaction dataset for collaborative object rearrangement. *arXiv*, 2024. 3, 6, 7, 8
- [68] Jianrong Zhang, Yangsong Zhang, Xiaodong Cun, Yong Zhang, Hongwei Zhao, Hongtao Lu, Xi Shen, and Ying Shan. Generating human motion from textual descriptions with discrete representations. In *Proceedings of the IEEE/CVF conference on computer vision and pattern recognition*, pages 14730–14740, 2023. 2
- [69] Mingyuan Zhang, Zhongang Cai, Liang Pan, Fangzhou Hong, Xinying Guo, Lei Yang, and Ziwei Liu. Motiondiffuse: Text-driven human motion generation with diffusion model. *arXiv preprint arXiv:2208.15001*, 2022. 1, 2
- [70] Lei Zhong, Chuan Guo, Yiming Xie, Jiawei Wang, and Changjian Li. Sketch2anim: Towards transferring sketch storyboards into 3d animation. *ACM Transactions on Graphics (TOG)*, 44(4):1–15, 2025. 2, 3, 4, 6, 7, 8
- [71] Lei Zhong, Yiming Xie, Varun Jampani, Deqing Sun, and Huaizu Jiang. Smoodi: Stylized motion diffusion model. In *European Conference on Computer Vision*, pages 405–421. Springer, 2025. 1, 2, 3
- [72] Yi Zhou, Connelly Barnes, Jingwan Lu, Jimei Yang, and Hao Li. On the continuity of rotation representations in neural networks. In *Proceedings of the IEEE/CVF conference on computer vision and pattern recognition*, pages 5745–5753, 2019. 3